Hindawi Publishing Corporation
Advances in Astronomy
Volume 2013, Article ID 429303, 10 pages
http://dx.doi.org/10.1155/2013/429303

Research Article

Diffusion Coefficients, Short-Term Cosmic Ray Modulation, and Convected Magnetic Structures

John J. Quenby,[1] Tamitha Mulligan,[2] J. Bernard Blake,[2] and Diana N. A. Shaul[1]

[1] *Blackett Laboratory, Imperial College, London SW7 2BZ, UK*
[2] *Space Sciences Department, The Aerospace Corporation, Los Angeles, CA 90009, USA*

Correspondence should be addressed to Tamitha Mulligan; tamitha.mulligan@aero.org

Received 2 August 2012; Revised 18 January 2013; Accepted 19 January 2013

Academic Editor: José F. Valdés-Galicia

Three cases of large-amplitude, small spatial-scale interplanetary particle gradients observed by the anticoincidence shield (ACS) aboard the INTEGRAL spacecraft in 2006 are investigated. The high data rates provided by the INTEGRAL ACS allow an unprecedented ability to probe the fine structure of GCR propagation in the inner Heliosphere. For two of the three cases, calculating perpendicular and parallel cosmic ray diffusion coefficients based on both field and particle data results in parallel diffusion appearing to satisfy a convection gradient current balance, provided that the magnetic scattering of the particles can be described by quasi-linear theory. In the third case, perpendicular diffusion seems to dominate. The likelihood of magnetic flux rope topologies within solar ejecta affecting the local modulation is considered, and its importance in understanding the field-particle interaction for the astrophysics of nonthermal particle phenomena is discussed.

1. Introduction

A Forbush Decrease (FD) is a global transient decrease in Galactic Cosmic-Ray (GCR) intensity followed by a substantially slower recovery. Since Scott Forbush's discovery and description of these phenomena in the late 1930s, FDs have been put into context with increasing developments within heliospheric physics. In particular, detailed observations of coronal mass ejections (CMEs) and in situ observations of the solar wind and energetic particles have greatly increased understanding of the underlying physics of FDs (see review articles by [1–3]).

This investigation focuses on small amplitude and high-frequency variability in the GCR corresponding to timescales less than a few hours, much shorter than that described by the classical FD. However, small-amplitude, mHz variability in the GCR is an experimental challenge in that very large instrumental geometric factors are required in order to make statistically significant measurements of the GCR in time periods of a few minutes or less. Therefore, only a few of these investigations can be found in the literature. Among these studies, [4] establishes the existence of short-spatial-scale GCR intensity gradients of a few percent amplitude (at >200 MeV energies) convecting with the solar wind past the Earth, coincident with the observation of an FD. This study correlates magnetic substructures within interplanetary CMEs (ICMEs) with short-scale intensity variations in the GCR. The authors in [5] investigate four simple magnetic field models for explaining short-term reductions in the GCR intensity and associated energetic particle propagation concluding that only a magnetic flux rope topology similar to that found in magnetic cloud ICMEs provides the magnetic conditions most likely to explain the overall depth of an FD.

Exploring the detailed relationship between particle intensity and magnetic field variability within the substructure of solar wind transients exhibiting large, short-period GCR fluctuations may yield new insight into energetic particle propagation within the Heliosphere. The authors of [6] originally derived energetic particle diffusion coefficients described by resonant wave scattering and field line wandering under the quasi-linear approximation. However, discrepancies of up to a factor four have been found by [7] in a strong scattering regime. In an attempt to represent observed conditions, the authors of [7] use coefficients derived empirically from solar particle propagation studies and numerical trajectory investigations in model solar wind

fields. Computational models solve the transport equation describing three-dimensional long-term GCR modulation by employing empirically justified diffusion coefficients, based on the goodness of fit to the overall spatial, temporal, and energy dependence of the modulation (e.g., [8]). However, these approaches do not attempt to relate the coefficients to in situ field data. A preferred method is the more direct derivation of the radial coefficient by McDonald et al. [9], who relate the radial gradient of the long-term modulation to the convective term directly.

In Section 2 of this paper, we discuss the instrumentation and data used in the analysis. In Section 3, we discuss the observations, first focusing on the particle observations and then focusing on solar wind observations and the connection with solar wind transients. In Sections 4 and 5, we use a version of the approach in [9] to estimate the diffusion coefficients locally and then compare the result with the prediction of quasi-linear theory. In Section 6, we present our conclusions.

2. Particle and Field Data

Particle data for this investigation is obtained from the large-area ACS of the SPI spectrometer mounted on the ESA INTEGRAL gamma-ray satellite. With a 24 R_E apogee, near continuous GCR monitoring is achieved. SPI consists of an array of 19 cooled Ge detectors, hexagonal in shape and of side 3.2 cm and height 7 cm [10]. The ACS is comprised of 91 bismuth germinate blocks. Several types of signals are available for GCR monitoring. The highest energy signals include the saturated counts of the ACS (ACSSAT) and the saturated counts of the Ge detector system (GEDSAT). Here "saturated" means that the amplitude from the energy deposited in the detector is sufficient to saturate the amplifier systems. The ACSSAT threshold is ~150 MeV [11]. The GEDSAT signal has an energy threshold of 200 MeV (a consequence of the energy required to penetrate the spacecraft shielding to reach the Ge detectors and subsequently lose an additional 10 MeV to the Ge detectors) [12].

In addition to ACSSAT and GEDSAT, the system has an ACS channel that counts all triggers in the system above ~100 keV. Much higher counting rates occur in this ACS channel because of the low-energy threshold. However, the lower-energy threshold also means that there are events in the run of the ACS data due to energetic magnetospheric electrons. Lucikly, ACS counts due to magnetospheric electrons have a spikey nature and time periods when they occur are easily identified and removed or ignored. The three INTEGRAL SPI channels, GEDSAT, ACSSAT, and ACS, make omnidirectional measurements with a broad and poorly known energy response. Since the GCR energy spectra peak in the energy range of hundreds of MeV per nucleon, this is not a serious issue. The compelling reason to use these INTEGRAL data is the stunning statistics provided by the relatively huge count rates that permit unprecedented temporal resolution of temporal changes in the GCR [4]. Solar wind magnetic field and plasma data are obtained from the MAG and SWEPAM instruments aboard the ACE spacecraft.

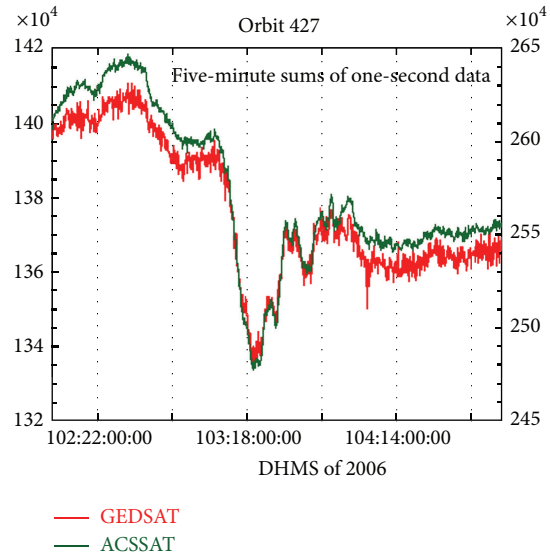

Figure 1: Five-minute sums of GEDSAT and ACSSAT count rates are plotted for Orbit 427.

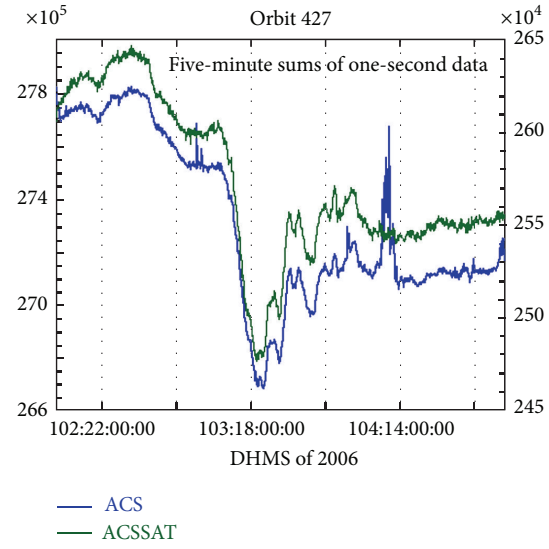

Figure 2: Five-minute sums of GEDSAT and ACSSAT count rates are plotted for Orbit 427.

3. Observations

3.1. GCR Study Intervals. Three periods of very rapid GCR intensity decrease were selected from 2006 INTEGRAL data, DOY 103 (orbit 427), DOY 117/118 (orbit 432), and DOY 1276/127 (orbit 435). Figure 1 compares the 5-minute sums of the GEDSAT and ACSSAT count rates for orbit 427 showing excellent agreement including the fine structure. The ACSSAT count rate is approximately twice that of the GEDSAT. Figure 2 similarly compares the ACS and ACSSAT rates. Excellent agreement is again found except for some spikes we ascribe to magnetospheric-related events. The orbits chosen for this analysis were selected based upon

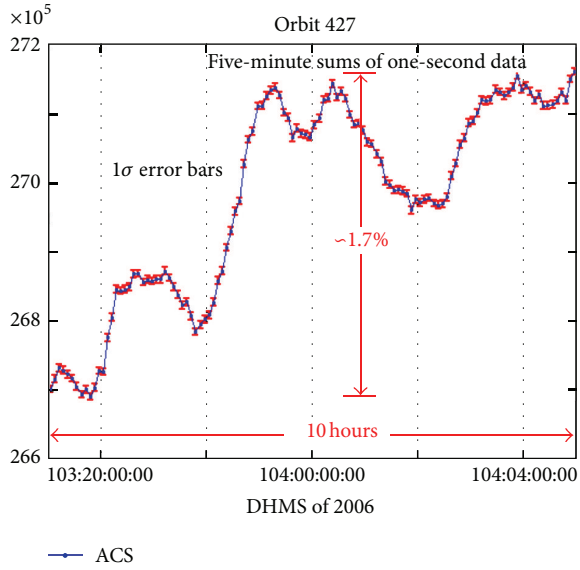

Figure 3: The data plotted in Figure 2 is replotted on expanded scales. The small size of the 1σ standard error bars reveals the statistical significance of the GCR variations.

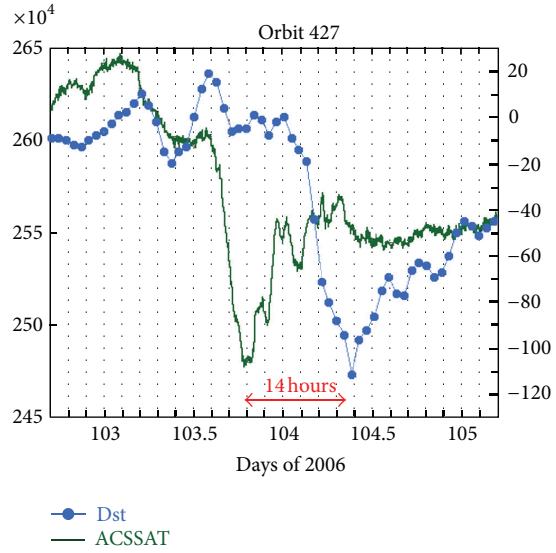

Figure 4: ACSSAT for Orbit 427 plotted with the time history of Dst.

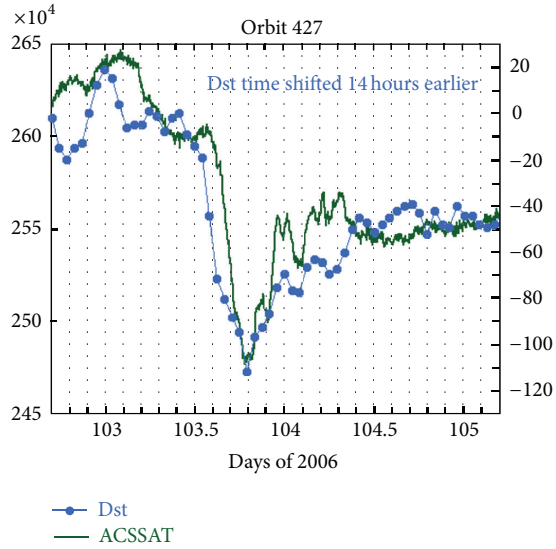

Figure 5: ACSSAT for Orbit 427 plotted with the time history of Dst shifted to earlier time by fourteen hours.

the striking short-term temporal changes in the GCR, and in the solar wind plasma and magnetic field. However the general tracking of the three channels lends confidence to the integrity of the measurement of the rapid flux variation.

The amplitude of the FD in which the sudden drop seen in both figures is encompassed is of magnitude ~3%. The extraordinarily large number of counts in 5-minute sums of the ACS data provides a marvelous statistical accuracy to the measurement of the GCR time history. Clearly many of the wiggles and bumps are real. Figure 3 illustrates this last point in more detail where conventional 1σ error bars are employed.

It has long been known that an FD has a similar time history to the evolution of Dst during the time period of the Forbush effect [13]. Sometimes they are nearly simultaneous while at other times there is a significant delay as was seen here (see Section 3.2 for more details on the Dst signature). To compensate for this effect, in Figure 4, we show the actual data for ACSSAT and Dst, while in Figure 5, Dst is shifted 14 hours earlier. The fact that such a time shift brings about a similarity in shape adds evidence for the convection model for the GCR-solar plasma structure over a time scale comparable to the duration of the rapid flux decrease studied.

Figure 6 plots the ACS data for orbit 427 along with the magnitude of the interplanetary field recorded by ACE. The field magnitude is seen to have increased abruptly at the time of the FD and remained high until the ACS recovered. This recovery did not return to pre-FD levels. (The spikes in the ACS count rate in this interval are due to leakage of magnetospheric electrons out of the radiation belts and can be safely ignored for this analysis.) To add to our confidence in the observed, rapid variability, we plot INTEGRAL in comparison with the lower statistical accuracy McMurdo neutron monitor data during the event in Figure 7.

3.2. Connection with Transient Solar Events. Looking at the solar wind data during this time shows the existence of an ICME. The interplanetary magnetic field and plasma conditions during a four-day period bracketing the ICME are shown in Figure 8. The bottom panel of the figure shows the ACS data. The transient spikes in the ACS data (occurring around midday of DOY 104) occur at the trailing boundary of the ICME indicated by the vertical lines. Note that the ACS data has not been time shifted to correspond to the particle signature observed at by ACE at the L1 Lagrangian point several hundred Re sunward of the Earth. The region prior to the ICME contains slow, cold plasma. The proton speed increases near the leading edge of the ICME, which causes a compression region, but no shock exists. In passing, we comment that

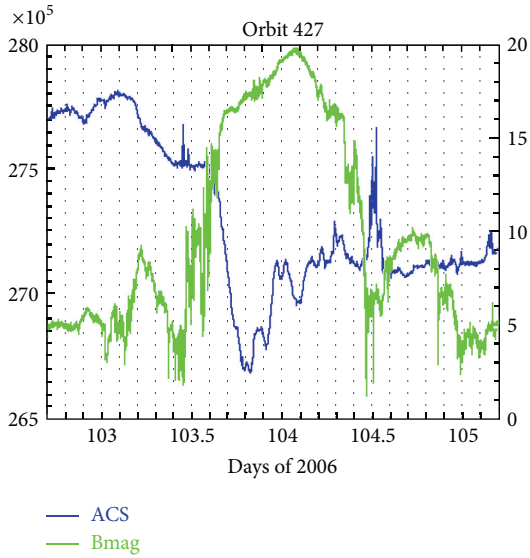

FIGURE 6: ACS is plotted for Orbit 427 along with the magnitude of the interplanetary field as seen by ACE.

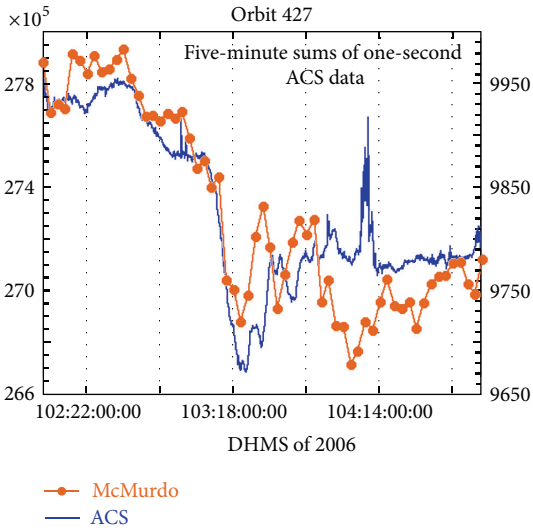

FIGURE 7: The ACS countrate is plotted with the countrate of the McMurdo neutron monitor for the time period of Orbit 427.

there is evidence that a shock front cannot be the basic cause of an FD. Close examination of the ICME reveals that the leading edge corresponds to the leading edge of the FD, but a simultaneous depression in Dst is not expected (see Figure 5) due to the presence of a strong northward component of the magnetic field (positive Bz) during the first half of the ICME. The drop in Dst is expected to occur when the field turns southward (negative Bz), which is some 12–15 hours after CME onset, consistent with the Dst drop shown in Figure 5.

A faster, warmer region is observed just downstream of the trailing ICME boundary. Taking a closer look at days 103 and 104 (04-13-06 and 04-14-06) shows some interesting details in the electron heat flux and ACS data during the period around the ICME. Inside the leading edge, sporadic bidirectional electron heat flux persists through the end of day 103, as shown in Figure 8. During this period, the heat flux has intermittent regions of unidirectional and bidirectional streaming indicating that the spacecraft is passing through alternately open and closed magnetic field lines in rapid succession. This changing topology may correspond to the short-period oscillations in the ACS count rates. It is difficult to assess the exact correspondence without first determining the time delay from L1 (ACE) to the location of INTEGRAL.

At the beginning of day 104 (Figure 8), the electron heat flux is primarily unidirectional but then switches to counter-streaming near the trailing end of the ICME (marked with a vertical line). It is also during this time that the plasma temperature increases, although the proton speed remains nearly constant. At the ICME trailing boundary, the magnetic field reaches a minimum and the field turns northward.

Figure 9 plots the ACS count rate over the period encompassing the three events studied, together with field components and magnitude, solar wind speed, temperature and density, and low-energy electron heat flux. The two vertical bands in the figure mark periods when a simple flux rope model may be fitted. The first is in good coincidence with the day 103 event but there is no simple rope configuration fitting the day 117/118 (ICME 2) or day 126/127 (ICME 3) events. At this stage, we are only able to say that the latter two events coincide with complex transient magnetic structures likely to exist over significant regions of space.

4. Derivation of the Quasi-Linear Diffusion Coefficients

The most basic derivation of the parallel diffusion coefficient can be found in [14]. We will first outline their approach because it both provides the most accessible expression to estimate this coefficient and illustrates the problems in any representation of the scattering in a realistic field model. The work of [14] assumes that particles follow helical trajectories along a nearly uniform field line, directed in the z direction, but suffer a series of small changes in pitch angle as they encounter transverse wave packets where the spatial wavelength of the wave along the field matches the projection of the cyclotron radius along the field. A perturbing force changes the parallel component of velocity and hence via conservation of the first adiabatic invariant, the pitch angle, depending on the spatial extent of the field perturbation. This extent of the wave-particle resonance is estimated as being within a spatial wave number range $\pm k_{||}/2$ where $k_{||} = \omega_B/v_{||}$ for gyrofrequency ω_B and particle velocity $v_{||}$ along field **B**. Random pitch angle scatters summing to 90° to achieve "reflection" and evaluated for an average pitch angle lead to a parallel diffusion coefficient, which we call the Kennel-Petscheck estimate $K_{||}^{K,P}$:

$$K_{||}^{K,P} = \frac{vVB^2}{12\pi P(f) f^2}, \tag{1}$$

where the resonant frequency $f = k_{||}V/2\pi$ for wind velocity V allows the particle gyration to match the spatial wavelength, and $P(f)$ is the power in waves perpendicular to **B**

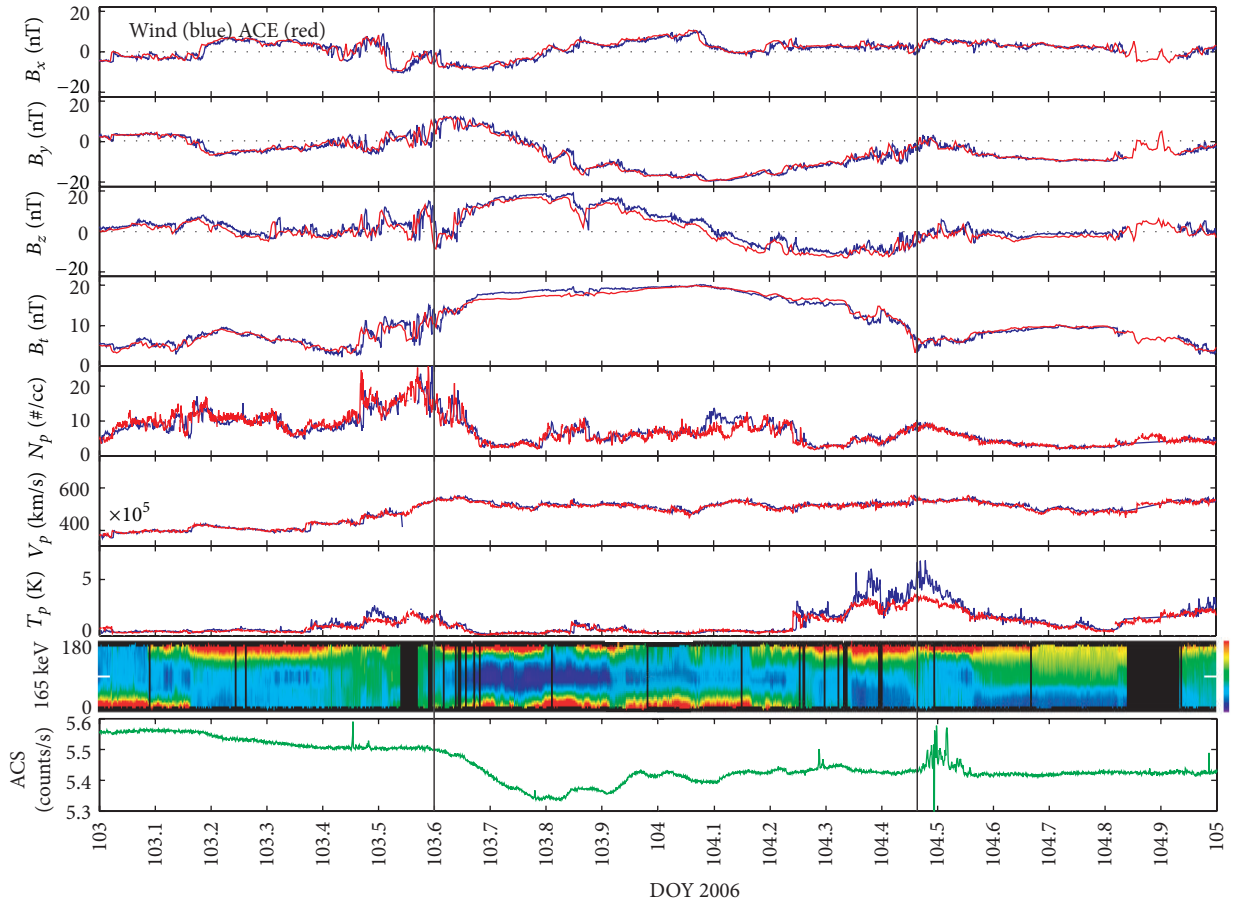

Figure 8: Wind and ACE IMF, plasma, and electron strahl (165 eV) data for 04-13 through 04-14 2006. INTEGRAL ACS data (unshifted) is shown in the bottom panel. The leading and trailing boundaries of the ICME are shown by vertical lines.

at f. The field model is known as a slab model where there is no dependence on x or y.

Even within the context of the assumption of transverse waves, the $K_{||}^{K,P}$ model fails to account in detail for the differing strength of scattering power at different pitch angles, and therefore the result must depend on spectral slope. Scattering at 90° is zero on the model because wave power falls to zero at very large $k_{||}$. A more general approach to finding the parallel diffusion coefficient, allowing the effects of waves and turbulence in three dimensions, starts with the Hall-Sturrock relation usually employed in a weakly turbulent field for the pitch angle diffusion coefficient $D_{\mu\mu}$ where μ is cosine of pitch angle:

$$D_{\mu\mu}(\mu) = Re\int_0^\infty d\epsilon \left\langle \frac{d\mu(t)}{dt}\frac{d\mu^\star(t+\epsilon)}{dt}\right\rangle. \quad (2)$$

Using the equation of motion for particles with unperturbed positions x and y with the mean field in z, the quasilinear approximation which picks out the dominant term perturbing the helical orbit leads to [15]

$$\frac{d\mu}{dt} = \frac{i\omega_B}{2^{0.5}B_\circ}\left(\left(1-\mu^2\right)^{0.5}\right) \times\left[\delta B_R(x(t))\,e^{i\Phi} - \delta B_L(x(t))\,e^{-i\Phi}\right], \quad (3)$$

where Φ is phase angle. Left- and right-handed polarisation is allowed for the wavelike parts of the perturbed field components:

$$\delta B_L = \frac{1}{2^{0.5}}\left(\delta B_x + i\delta B_y\right),$$
$$\delta B_R = \frac{1}{2^{0.5}}\left(\delta B_x - i\delta B_y\right). \quad (4)$$

Various models are then chosen which define the perturbed fields via Fourier transforms representing the wave motion or turbulent, convected field structure. The integral to be performed in (2) picks out the resonance of the stationary wave and convected structure patterns with the helical orbit. Here we concentrate on the simplest or slab model which attributes the perturbations to Alfven waves propagating with k vectors parallel to the mean field which means that all change is in x or y. In [6], it was then found that

$$\frac{\left\langle(\Delta\mu)^2\right\rangle}{\Delta t} = \frac{\left(1-\mu^2\right)}{|\mu|\,v}\frac{e^2V}{m^2c^2}P_{xx}\left(f = \frac{V\omega_\circ}{2\pi\mu v}\right), \quad (5)$$

where $m = \gamma m_\circ$ and $\omega_\circ = eB/mc$, γ is the Lorenz factor, and $P_{xx} = \delta/f^n$ is here the power in one perpendicular component with f running from $-\infty$ to $+\infty$. A parallel diffusion

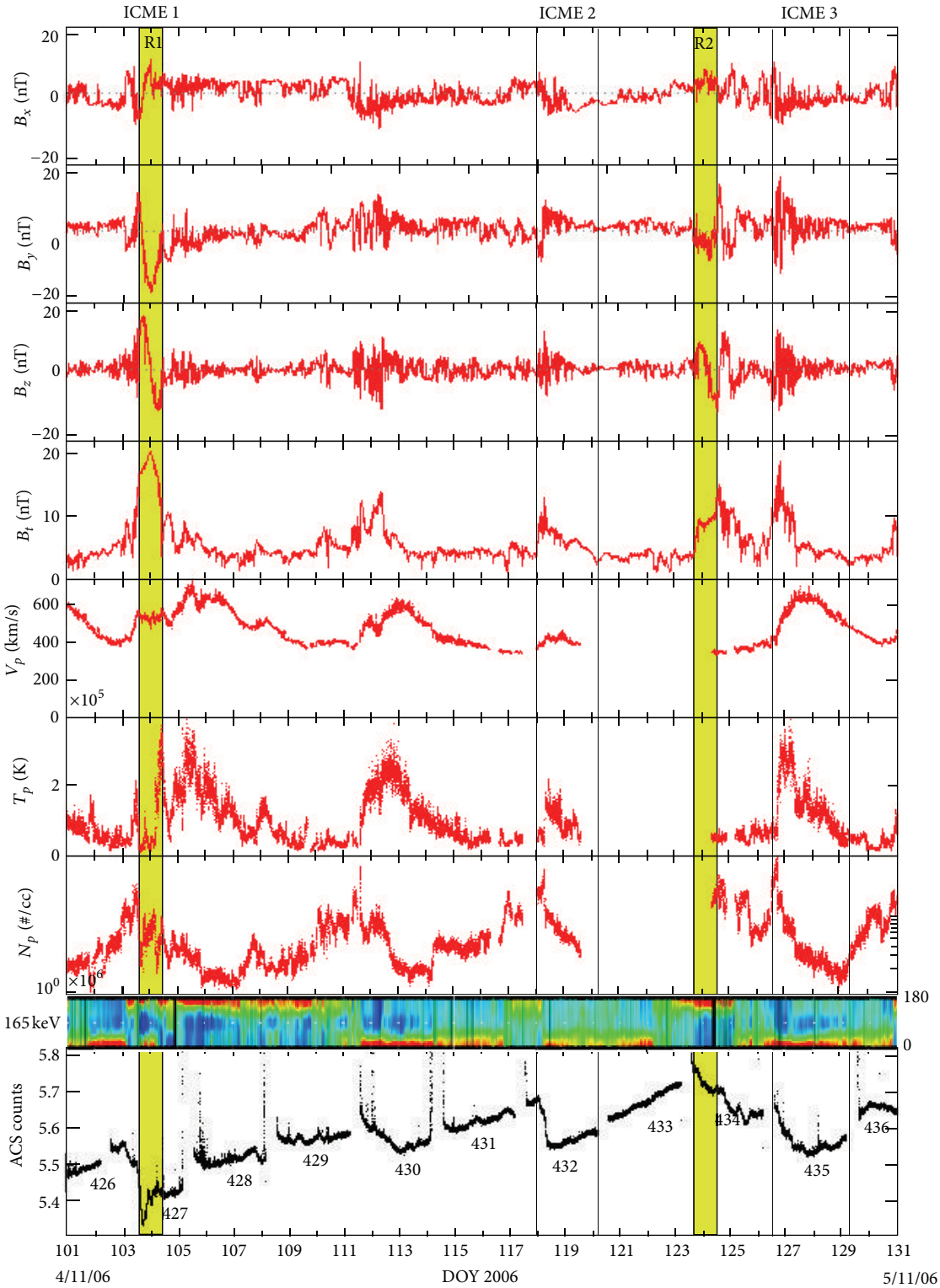

Figure 9: ACS count rate over entire period encompassing the three ICME events studied together with solar wind field and plasma components from ACE and electron strahl from Wind. Highlighted regions indicate presence of flux ropes.

coefficient is then obtained by studying the relaxation of a small anisotropy in pitch angle space and Hasselmann and Wibberenz [16] obtain

$$K_{||} = \frac{v^2}{2}\int_{-1}^{1}\left[\int_{0}^{\mu'}\frac{1-\mu^2}{\left\langle(\Delta\mu)^2\right\rangle/\Delta t}d\mu\right]\mu' d\mu'. \quad (6)$$

Substituting (6) into (5) yields (e.g., [17])

$$K_{||}^{HW} = v^{3-n}V^{n-1}\frac{B^2}{(2\pi)^n}\frac{\omega_\circ^{n-2}}{\delta}\frac{1}{(4-n)(2-n)}. \quad (7)$$

The symbol δ is the coefficient arising from one of three field components obtained in a Fourier transform, and it is assumed that perpendicular power dominates power in the field magnitude. Note that axial symmetry has been assumed for the perturbation spectrum and also that the cyclotron radius of the scattered particles lies in a range of spatial wave frequencies which can be described by a single power law. This assumption is satisfied by the particle and magnetic data used subsequently in this work.

Under the approximation that the power spectrum of transverse fluctuations was proportional to f^{-1}, the author's result (6) leads to a $K_{||}$ value which is close to (1) and has been commonly used in the past. While values of $n \approx 1.1$ have been found during disturbed periods, a Kolmogorov-like value of 5/3 is more usual.

Subsequent work, on $K_{||}$, realised that the quasi-linear theory employed did not produce scattering through 90° pitch angles. However, Alfvenic waves propagating at a variety of angles to the mean field are found in the Solar Wind, and also compressional, longitudinal waves may provide 10% of the fluctuation power. Moreover, rotational discontinuities may occur several times in a CME. All these disturbances can provide "mirroring" to particle propagation where the pitch angle relative to the mean field is near 90°. Hence the scattering mechanism at large pitch angles may be the dominant influence on the rate of diffusion, and because such corrections to quasi-linear theory tend to decrease $K_{||}$ (e.g., [18]), (7) could be treated as an upper limit [18], unless most turbulence is purely Alfvenic with $|\mathbf{B}|$ preserved so that scattering at large angle is only due to a small, compressive component of the field turbulence. However, the authors of [19] introduce a two-component field model, one describing the slab approximation and the second an axisymmetric power spectrum describing variations perpendicular to the mean field. Different correlation lengths are introduced for the two components. These workers compared the quasi-linear result (QLT) and their two component model, based on average solar wind conditions at 1 AU with the "Palmer Consensus" mean free paths, as determined by a compilation of determinations from particle propagation. They found that a model with 90% of power corresponding to the slab model gave $\lambda_{||}$ in the ~100 MV range at the bottom of the "Palmer" range while a model with 90% of the power concentrated in perpendicular direction fluctuations laid a factor three higher, at the top of the "Palmer" range. While the results of [19] might encourage us to believe that our use of QLT may be only a factor two to three in error, previous numerical simulations by [7] appeared to confirm a series of investigations suggesting a larger underestimate (e.g., [17]). In [7], a field model was employed whereby each short segment of particle trajectory experienced a field obtained from actual B and V measurements as the wind flowed past a spacecraft. An equilibrium pitch angle distribution was then set up by numerically following particles within the field model after injection and until removal at boundaries. The slope of the distribution function in pitch angle space then gave $D_{\mu\mu}$. Solar particle propagation data used to deduce the spatial diffusion coefficient came from a contemporary solar particle event. The use of (7) gave an estimate a factor 8 less than that derived from the particle data and a factor 4 less than that obtained by the numerical model.

The approximation of (7) applies to an axisymmetric slab model of transverse fluctuations with no net polarisation and varying only parallel to the mean field, and we assume that corrections due to a finite Alfven speed, as implied in the equations of motion of [15], can be neglected because the particles move close to c. Our subsequent use of (7), motivated by the complexity of the subsequent approaches which are beyond the scope of this paper, must be tempered by the knowledge that it is very likely to only represent a lower limit.

Concerning perpendicular diffusion, we again start by describing the well-known and easily accessible approximation, before mentioning analytical improvements to the theory and computational approaches which will allow an assessment of the error involved with the adopted equation. Since particles of small Larmor radii compared with the dominant scale of field fluctuations attempt to follow field lines, it is not surprising that deviation from a mean direction is thought of as a combination of motion of guiding centers following wandering field lines and diffusive scattering perpendicular to these lines. In [6], it was found that the dominant cause for perpendicular diffusion lays in the power at spatial frequencies of the turbulence approaching zero, $P_{xx}(f = 0)$, corresponding to the description of field line wandering. Resonance scattering similar to that described in the pitch angle case was found by Jokipii [6] to be relatively small. The result given for the perpendicular displacement $\langle\delta x\rangle$ at cosine pitch angle μ was

$$\frac{\left\langle\delta x^2\right\rangle}{\delta t} = \frac{\mu v V P_{xx}(f=0)}{B_\circ^2}. \quad (8)$$

Later, Foreman et al. [20] reevaluated this result and quote

$$K_\perp = 4\times10^{20}\left(\frac{v}{c}\right)\ \mathrm{cm}^2,\ \mathrm{sec}^{-1} \quad (9)$$

for $P_{x,x}(f = 0) = 4\times10^{-6}$ Gauss^2/Hz longitudinal power, $V = 4\times10^7$ cm/sec, and $B = 4\times10^{-5}$ Gauss. We shall use (9), scaled to fit the actual field and wind parameters, according to (8).

Subsequent analytical work, especially [21], finds that the interplay between parallel and perpendicular scattering can suppress the perpendicular motion, for example, if the reversal along the field allows the gyromotion to cause the particle

to sample field lines closely similar to those encountered before the scatter of parallel motion. Matthaeus et al. [21] define $K_\perp$ according to the Taylor-Green-Kubo formulation which in their case they write as

$$K_{xx} = \frac{a^2}{B_\circ} \int_0^\infty dt' \left\langle v_z(0)\, v_z\left(t'\right)\right\rangle \times \left\langle b_x\left[x(0), 0\right] b_x\left[x\left(t'\right), t\right]\right\rangle. \tag{10}$$

It has been assumed that the relation between the perpendicular velocity and the perpendicular field perturbation, assuming axial symmetry, is

$$v_x(t) = \frac{a v_z(t)\, b_x\left[x_m(t)\right]}{B_\circ}, \tag{11}$$

where x_m is a mean of the gyromotion. This formula clearly describes motion following wandering field lines if $a = 1$, but in the work based on the approach outlined, a value $a = 1/3$ is taken as fitting numerical simulations corresponding to the analytical model adopted, and no theoretical justification seems to be supplied as yet for the value of the constant.

The work of [22] is the most recent and general analytical approach to finding $K_\perp$ in a medium of arbitrary turbulence, without the restrictions of, for example, the slab model or the two component model mentioned before. His nonlinear model leads to the following expression involving the power spectrum with arbitrary propagation vector $P_{xx}(\mathbf{k})$:

$$K_\perp = \frac{a^2 v^2}{3B_\circ^2} \int d^3k \frac{P_{xx}(\mathbf{k})}{A(\mathbf{k}) + (4/3) K_\perp k_\perp^2 + v/\lambda_{||}}, \tag{12}$$

where

$$A(\mathbf{k}) = \frac{\left(v k_{||}\right)^2}{3 K_\perp k_\perp^2}. \tag{13}$$

Suppressing the effects of parallel scattering allows this equation to tend to the field line wandering limit while restricting the power spectra to slab and axisymmetric perpendicular disturbance allows the results of [21] to be recovered. In a 3D turbulence model, the interplay of parallel and perpendicular effects is illustrated by considering the terms after the integral sign.

An alternative approach to incorporating 3D turbulence lies in computations similar to those described in [7]. The authors of [23] suppress variability in one of the three dimensions, so that $\mathbf{B}(x,y)$ is constant in z. Diffusion in z due to field fluctuations in the x-y plane was measured again by numerically tracking particles again in a steady-state experiment while drift in z was measured by following the time evolution of the distribution function. The numerical experiment had deliberately suppressed field line wandering in z. The result was a $K_\perp$ of similar magnitude to the field line wandering estimate. Net drift was consistent with the combined effects of field gradient and curvature drifts due to the x-y plane variability averaged over the one day sample used, calculated on guiding center theory. Our conclusion is that employment of (9) could result in approximately a factor of two underestimate.

In applying the aforementioned expressions to field data, we employ ACE 4-minute component averages, using 0.71 of a day's data for convenience relating to the Matlab algorithm employed. We obtain the power in a typical perpendicular component by doing fast Fourier transforms to find the power in solar radial, tangential, and normal components as a function of frequency and then finding the sum of resolving each component in a direction perpendicular to the mean field. Power laws are used to fit these summed components. Field magnitudes are found from averages of the 4-minute total field magnitudes because the particles are actually attempting to follow the fluctuation field direction, rather than the mean field over 0.71 of a day. Solar wind data from ACE is used to determine the mean flow velocity of each selected period. Applying the aforementioned results to the field/plasma data of DOY 103, 2006 and the pairs of DOY 117, 118 and 126, 127 yields for 200 MeV protons the results of Table 1. Here ψ is the mean field-radial direction angle. It is noteworthy that the perpendicular power spectra with a negative slopes up to 1.7 are obtained, considerably steeper than for the $n = 1$ assumed in (1). Hence the scattering at high pitch angles is less effective and $K_{||}^{K,P}$ is likely to be an underestimate.

5. Diffusion Coefficients, the GCR Gradient, and Short-Term Modulation

The maximum GCR drop in intensity during day 103 occurs between 103.6 and 103.8 Assuming that this is due to spatial convection of the feature, as is likely from previous studies of such events [4], the radial spatial gradient of the ACSSAT intensity is 3.43×10^{-14}/cm or 52 percent/AU, corresponding to 200 MeV GCR.

If we assume that a quasi-equilibrium is still maintained between convective outflow, adiabatic energy loss, and diffusive inflow,

$$CVU = -\left(K_{||}^{\mathrm{cr}} \cos^2\chi + K_\perp^{\mathrm{cr}} \sin^2\chi\right) \frac{\partial U}{\partial r}, \tag{14}$$

where C is the Compton-Getting factor appropriate to the differential number density spectrum, U, at 200 MeV and χ is the field-radial direction angle. $C = 0.81$ close to the previous solar minimum, while $\chi = 68^\circ$ on average during the interval of the rapid GCR decrease. We will now separately investigate whether parallel or perpendicular diffusion is the most important in maintaining the assumed quasi-equilibrium with small radial streaming by successively ignoring each term on the right-hand side of the above. Putting in values yields

$$K_{||}^{\mathrm{cr}} = 8.4 \times 10^{21}\ \mathrm{cm}^2,\ \mathrm{sec}^{-1},$$
$$K_\perp^{\mathrm{cr}} = 1.4 \times 10^{21}\ \mathrm{cm}^2,\ \mathrm{sec}^{-1}. \tag{15}$$

Similar estimates are made for the other events, days 117/118 and 126/127. These cosmic-ray-derived diffusion coefficients, $K_{||}^{\mathrm{cr}}$ and $K_\perp^{\mathrm{cr}}$, are also entered in Table 1. For DOY 103,

Table 1: Diffusion coefficients obtained from power spectra and particle gradients in cm^2, sec^{-1}.

	DOY 103	DOY 117	DOY 118	DOY 126	DOY 127
$K_{\|\|}^{K,P}$	6.3×10^{20}	9.66×10^{20}	2.41×10^{20}	1.0×10^{20}	3.40×10^{20}
$K_{\|\|}^{H,W}$	5.5×10^{21}	9.39×10^{21}	2.8×10^{21}	1.7×10^{21}	1.99×10^{21}
$K_{\perp}$	4.1×10^{20}	1.38×10^{20}	1.71×10^{20}	1.54×10^{21}	1.12×10^{21}
ψ	68	24.8	45.5	75.8	45.7
$K_{\|\|}^{\mathrm{cr}}$	8.4×10^{21}	1.1×10^{21}	2.19×10^{21}	3.73×10^{22}	7.13×10^{21}
$K_{\perp}^{\mathrm{cr}}$	1.4×10^{21}	5.17×10^{21}	2.15×10^{21}	2.39×10^{21}	6.79×10^{21}

and assuming the validity of the power spectral-based estimates, neither the perpendicular diffusion value nor the simple, $K_{||}^{K,P}$ parallel diffusion case can satisfy the quasi-equilibrium. However, because the field-based $K_{||}^{H,W}$ and gradient-based, $K_{||}^{\mathrm{cr}}$ estimates are close, parallel diffusion seems to satisfy quasi-equilibrium. For the event of days 117/118 parallel diffusion again seems to give a better agreement between power spectrum calculated and gradient-derived diffusion coefficients, especially as the major part of the observed sharp decrease best corresponds to day 118 power spectral analysis. However for the event of days 126/127, perpendicular diffusion seems to give a little better accord, especially as the major drop lies around the day 126/127 boundary. Note the high ψ angle on day 126 which might indicate the reason for the dominance of perpendicular diffusion. On the other hand, previously noted, marked discrepancy between quasi-linear theory and diffusion computations based on actual field values may be in play here.

Inspection of Figure 8, Section 3.2, shows a rapid field rotation at the time of the rapid decrease with radial component going through zero and with the dominant field component normal to the ecliptic in the event of day 103. It is possible to imagine that nearer the sun the GCR intensity was significantly reduced by a field configuration unfavourable to radial diffusion. This allowed a new quasi-equilibrium to be set up with inflow from a large angle to the ecliptic plane and radial direction from some entry point at the boundary of the traveling large magnetic disturbance. What we see during the three events is the quasi-equilibrium expressed by (14) as it is convected past the Earth. The short-term modulation under consideration here is thus essentially due to a barrier mechanism, because true radial diffusion is largely inhibited during the events.

All three field components exhibit large changes but only one event clearly fits a flux rope model. A bidirectional heat flux persisting through to the end of day 103 has already been noted. We have already discussed the flux rope as a suitable GCR barrier [4, 5], although the detail of the proposed mechanism is different here.

6. Conclusions

We have set out to demonstrate the likely validity of a model for significant short-term reduction of the GCR intensity and the use of this model to obtain information on energetic particle diffusion. Approximate theoretical values of the parallel and perpendicular diffusion coefficients have been obtained appropriate to the actual field turbulence present at the time of passage of three selected events. Reference to previous analytical and Monte Carlo numerical studies taking into account 2- or 3-dimensional field representations, not present in the slab approximation of the adopted calculation of the coefficients, allowed an assessment of errors in our procedure to be made. A sufficiently satisfactory explanation of the three events was provided by the idea of a quasi-equilibrium field/particle structure being convected past the Earth with a single, dominant mode of diffusive propagation, either parallel or perpendicular to the mean field of the event. Reasonable self-consistency between diffusion coefficients derived by particle gradient and analytic theory was achieved. Nevertheless, there is every reason to urge the application of more comprehensive modeling, for example, by the methods of [7, 19, 22], to better check the extent of this agreement.

Three-dimensional models of the overall heliospheric modulation assume diffusive scattering varying smoothly over large spatial scales with at most a dependence on angle with respect to the solar equatorial plane. The relative importance of this, near isotropic and homogeneous turbulence model, compared with barrier effects discussed in this work must depend on the abundance of flux rope magnetic topologies within the solar wind.

In terms of the wider, astrophysical significance, the method proposed here of using local particle conditions to check diffusion coefficients with locally derived plasma parameters seems unprecedented as a way of validating the ability to model cosmic wave-particle interaction in a collisionless regime. One only has to point to the extensive use made of quasi-linear theory for the interaction in nonthermal astrophysical shock modeling to appreciate the worth of the investigation.

Acknowledgments

D. N. A. Shaul acknowledges Science & Technology Facilities Council (STFC) support. T. Mulligan and J. B. Blake acknowledge the support for this work under NASA Grant CG189307NGA. The authors would like to thank the INTEGRAL team for supplying the INTEGRAL data, the ACE MAG and SWEPAM teams for making their data available on the ACE Science Center website (http://www.srl.caltech.edu/ACE/ASC/), and the Wind 3DP team for making their data available on the WIND 3-D Plasma and Energetic Particle Investigation Web site (http://sprg.ssl.berkeley.edu/wind3dp/esahome.html).

References

[1] J. A. Lockwood, "Forbush decreases in the cosmic radiation," *Space Science Reviews*, vol. 12, no. 5, pp. 658–715, 1971.

[2] H. V. Cane, "Coronal mass ejections and forbush decreases," *Space Science Reviews*, vol. 93, no. 1-2, pp. 55–77, 2000.

[3] I. G. Richardson, "Energetic particles and corotating interaction regions in the solar wind," *Space Science Reviews*, vol. 111, no. 3-4, pp. 267–376, 2004.

[4] T. Mulligan, J. B. Blake, D. Shaul et al., "Short-period variability in the galactic cosmic ray intensity: high statistical resolution observations and interpretation around the time of a Forbush decrease in August 2006," *Journal of Geophysical Research A*, vol. 114, no. 7, Article ID A07105, 2009.

[5] J. J. Quenby, T. Mulligan, J. B. Blake, J. E. Mazur, and D. Shaul, "Local and nonlocal geometry of interplanetary coronal mass ejections: galactic cosmic ray (GCR) short-period variations and magnetic field modeling," *Journal of Geophysical Research*, vol. 113, no. A10, 2008.

[6] J. R. Jokipii, "Cosmic-ray propagation. I. Charged particles in a random magnetic field," *The Astrophysical Journal*, vol. 146, p. 480, 1966.

[7] J. F. Valdés-Galicia, G. Wibberenz, J. J. Quenby, X. Moussas, G. Green, and F. M. Neubauer, "Pitch angle scattering of solar particles: comparison of "particle" and "field" approach—I. Strong scattering," *Solar Physics*, vol. 117, no. 1, pp. 135–156, 1988.

[8] U. D. Langer, M. S. Potgieter, and W. R. Webber, "Modelling of "barrier" modulation for cosmic ray protons in the outer heliosphere," *Advances in Space Research*, vol. 34, no. 1, pp. 138–143, 2004.

[9] F. McDonald, Z. Fujii, P. Ferrando et al., "The cosmic ray radial and latitudinal intensity gradients in the inner and outer heliosphere 1996-2001.3," in *Proceedings of the 27th International Cosmic Ray Conference (ICRC'01)*, vol. 10, p. 3906, Hamburg, Germany, August 2001.

[10] G. Vedrenne, J. P. Roques, V. Schönfelder et al., "SPI: the spectrometer aboard INTEGRAL," *Astronomy and Astrophysics*, vol. 411, no. 1, pp. L63–L70, 2003.

[11] P. Jean, G. Vedrenne, J. P. Roques et al., "SPI instrumental background characteristics," *Astronomy and Astrophysics*, vol. 411, no. 1, pp. L107–L112, 2003.

[12] B. J. Teegarden, J. Naya, H. Seifert et al., "SPI: a high resolution imaging spectrometer for INTEGRAL," in *Proceedings of the 4th Compton Symposium*, C. D. Dermer, M. S. Strickman, and J. D. Kurfess, Eds., vol. 410 of *AIP*, 1997.

[13] K. Kudela and R. Brenkus, "Cosmic ray decreases and geomagnetic activity: list of events 1982–2002," *Journal of Atmospheric and Solar-Terrestrial Physics*, vol. 66, no. 13-14, pp. 1121–1126, 2004.

[14] C. F. Kennel, H. Petscheck, and H. E, "Limit on stably trapped particle fluxes," *Journal of Geophysical Research*, vol. 71, no. 1, pp. 1–28, 1966.

[15] A. Teufel and R. Schlickeiser, "Analytic calculation of the parallel mean free path of heliospheric cosmic rays: I. Dynamical magnetic slab turbulence and random sweeping slab turbulence," *Astronomy and Astrophysics*, vol. 393, no. 2, pp. 703–715, 2002.

[16] K. Hasselmann and G. Wibberenz, "A note on the parallel diffusion coefficient," *The Astrophysical Journal*, vol. 162, p. 1049, 1970.

[17] J. J. Quenby, G. E. Morfill, and A. C. Durney, "The solar proton diffusion mean free path and the anisotropic particle event of November 18, 1968," *Journal of Geophysical Research*, vol. 79, no. 1, pp. 9–16, 1974.

[18] M. L. Goldstein, "The mean free path of low-rigidity cosmic rays," *Journal of Geophysical Research*, vol. 85, no. A6, pp. 3033–3036, 1980.

[19] A. Shalchi, J. W. Bieber, W. H. Matthaeus, and R. Schlickeiser, "Parallel and perpendicular transport of heliospheric cosmic rays in an improved dynamical turbulence model," *Astrophysical Journal*, vol. 642, no. 1, pp. 230–243, 2006.

[20] M. A. Foreman, J. R. Jokippi, and A. J. Owens, "Cosmic-ray streaming perpendicular to the mean magnetic field," *The Astrophysical Journal*, vol. 192, pp. 535–540, 1974.

[21] W. H. Matthaeus, G. Qin, J. W. Bieber, and G. P. Zank, "Nonlinear collisionless perpendicular diffusion of charged particles," *Astrophysical Journal Letters*, vol. 590, no. 1, pp. L53–L56, 2003.

[22] A. Shalchi, "A unified particle diffusion theory for cross-field scattering: subdiffusion, recovery of diffusion, and diffusion in three-dimensional turbulence," *Astrophysical Journal Letters*, vol. 720, no. 2, pp. L127–L130, 2010.

[23] X. Moussas, J. J. Quenby, and J. H. Valdes-Galicia, "Drift motion and perpendicular diffusion of energetic particles in interplanetary space based on spacecraft data," *Astrophysics and Space Science*, vol. 86, no. 1, pp. 197–207, 1982.